

www.acsmaterialsletters.org

Controlling the Lithium-Metal Growth To Enable Low-Lithium-Metal-Excess All-Solid-State Lithium-Metal Batteries

Ming Liu, $^{\nabla}$ Chao Wang, $^{\nabla}$ Zhu Cheng, Swapna Ganapathy, Lucas A. Haverkate, Sandeep Unnikrishnan, and Marnix Wagemaker*



See https://pubs.acs.org/sharingguidelines for options on how to legitimately share published articles

Downloaded via TNO on August 6, 2021 at 12:46:42 (UTC).

Cite This: *ACS Materials Lett.* 2020, 2, 665–670



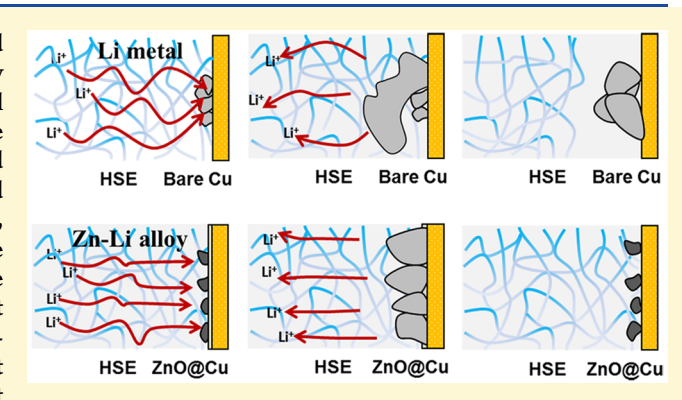
ACCESS I

III Metrics & More

Article Recommendations

s Supporting Information

ABSTRACT: Solid-state lithium-metal batteries are considered to be promising candidates for next-generation high-energy density storage devices to power electrical vehicles. Critical challenges for solid-state lithium-metal batteries include the large morphological changes associated with the plating and stripping of lithium metal and decomposition of the solid electrolyte, because of the reductive nature of the lithium metal, both increasing the lithium metal—solid electrolyte interface resistance. This is especially challenging when starting in the discharged state with a bare anode or "anode-less" current collector facing the solid electrolyte. To overcome this, a 100-nm thin layer of ZnO is deposited on the copper current collector with atomic layer deposition (ALD). During the first



charge, this results in more homogeneous lithium-metal growth, rationalized by the formation of a Zn-Li alloy that acts as seed crystals for the lithium metal. The resulting more homogeneous lithium-metal growth maintains better contact with the solid electrolyte, leading to more reversible cycling of lithium metal. Minor prelithiating of the ZnO/Cu anode with 1 mAh/cm² further improves the cycling performance, as demonstrated in a full all-solid-state cell using LiFePO₄ as a cathode, resulting in an average Coulombic efficiency of >95%. These findings mark the first steps in an interface strategy to overcome the challenges at the solid electrolyte/lithium-metal interface in solid-state lithium-metal batteries.

roposed by Whittingham in 1976,1 the lithium metal battery (LMB) makes use of the high specific capacity (3860 mAh g^{-1}) and low reduction potential (-3.040 V vs SHE) of lithium metal, motivating the current intensive research toward this "Holy Grail" anode for lithium batteries.^{2,3} Unfortunately, the severe reactivity of lithium metal with liquid electrolytes, leading to uncontrolled solid electrolyte interface (SEI) growth, as well as the formation of dendritic lithiummetal morphologies result in a short cycle life and safety concerns that have hindered the capitalization of lithiummetal-based batteries (LMBs).3-7 Specifically, when, during plating, the current exceeds the supply of Li ions, determined by the conductivity of the electrolyte, ion depletion at the Li metal surface occurs after the characteristic Sand's time.^{3,7} Under these conditions, plating becomes inhomogeneous and self-amplified growth of dendrites is induced. Even at lower current densities, dendritic growth is induced, presumably because of the inhomogeneous nature of the SEI.^{3,8} As a consequence, the use of volatile and flammable liquid organic

electrolytes in lithium-metal batteries leads to significant safety concerns. $^{9-11}\,$

In this context, replacing the liquid electrolyte with a solid electrolyte (SE) is considered to be a promising strategy. In addition to the challenges related to the electrochemical stability of the solid electrolytes, this also introduces a different challenge, compared to liquid electrolytes: How to maintain contact between the SE and the lithium-metal anode to guarantee Li-ion transport, especially because the lithium metal undergoes large volumetric and morphological changes upon (dis)charging. The interface should thus provide high ionic conductivity, resist the reducing potential of lithium-

Received: April 15, 2020 Accepted: May 14, 2020 Published: May 14, 2020





metal environment, and prevent delamination upon the inherent lithium-metal volumetric change upon cycling. 15,16 From the many solid electrolytes developed^{3,17,18} so far, only poly(ethylene oxide) (PEO)-based polymer electrolytes, developed by Delmas, have allowed the development of commercial solid-state lithium-metal batteries. 19 However, the disadvantage is the relatively low conductivity of polymerbased electrolytes, which demands battery operation above 60 °C. Aiming at more-challenging room-temperature lithiummetal batteries, countless strategies have been developed to improve the ionic conductivity, interfacial properties, and the safety issues related to lithium metal in polymer-based batteries. 12-14,20-23 This has resulted laboratory-scale lithium-metal batteries operating at room temperature, however, typically starting with thick lithium metal sheets at the anode. ^{12–14,20–23} In practice, a large excess of lithium at the copper current collector reduces the energy density of the LMB and makes battery assembly more costly and challenging. 24,25 Ideally, all active Li is initially stored in the cathode to maximize the energy density. However, starting with a bare copper current collector in contact with the solid electrolyte makes it extremely challenging to maintain this contact, to support Li-ion transport during cycling,³ upon the lithium-metal growth and shrinking. To the best of our knowledge, only Yang et al.¹² have demonstrated cycling of a Cu/solid electrolyte interface in a solid-state Li-Cu battery, which was achieved by e-beam deposition of copper at the bottom of a garnet skeleton, where the lithium-metal plating occurs in the porous garnet matrix. However, it was stressed that completely stripping lithium metal from the copper current collector should be avoided, because this could extract Li from the Li₇La₃Zr₂O₁₂ (LLZO) electrolyte itself and lead to collapse of the LLZO structure. 12 This demonstrates the challenges to achieve reversible cycling of lithium-metal solidstate batteries starting with a lithium-metal-free anode, especially aiming for easy-to-produce, future high-energydensity LMBs.

Here, we demonstrate the formation of large lithium deposits on the bare copper current collector in a solid-state LMB, utilizing a PEO-based HSE previously reported, 14 upon cycling at room temperature. The large deposits result in contact loss, increase the impedance, and cause these cells to fail within a few cycles. In order to improve the compatibility between the HSE and the copper current collector, a thin layer of ZnO was coated on copper via atomic layer deposition (ALD). Upon plating, this forms a LiZn alloy, making the surface lithium-philic, resulting in more evenly distributed lithium-metal deposits, rationalized by the larger number of lithium-metal nucleation sites. The improved cycling of the lithium-metal plating and stripping was evaluated by operando neutron depth profiling (NDP), monitoring the lithium density, as a function of depth on the copper current collector. A much-higher lithium efficiency and better lithium geometry is observed. Finally, a full cell composed of a 3 mg/cm² LiFePO₄ cathode and a 1 mAh/cm² prelithiated ZnO@Cu anode was successfully combined with a high Coulombic efficiency, illustrating the potential of this interface strategy for the development of solid-state lithium-metal batteries.

In order to explore the Li deposition morphology on a bare copper current collector, a solid-state Cu/HSE/lithium-metal battery is assembled. The HSE is composed of PEO, lithium bis(trifluoromethanesulfonyl)imide (LiTFSI), succinonitrile (SN), and $\text{Li}_{1.5}\text{Al}_{0.5}\text{Ge}_{1.5}(\text{PO}_4)_3$ (LAGP) as prepared pre-

viously, ¹⁴ in which Li-ion transport was enhanced through concurrent transport in both the organic and inorganic phases. The resulting conductivity, 1.73×10^{-4} S/cm, enables room-temperature battery cycling. ¹⁴ The electrochemical performance of the Cu/HSE/Li battery cycled at 0.05 mA/cm² for 4 h is shown in Figure 1a. The poor electrochemical performance

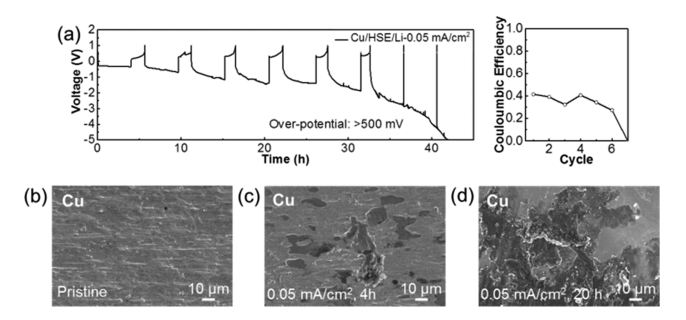


Figure 1. Plating lithium metal at the Cu/HSE interface. (a) Electrochemical performance of Cu/HSE/Li batteries at 0.05 mA/cm 2 for 4 h. (b, c, d) SEM measurements showing the fresh Cu, 0.2 and 1 mAh/cm 2 Li plated metal morphology in a Cu/HSE/Li battery.

of the Cu/HSE/Li battery, as expressed by the large overpotential (~500 mV) and poor Coulombic efficiency (~40%), illustrates the difficulty involved in plating lithium metal on the bare copper surface facing the HSE. The large polarization in the end indicates that delamination of the electrode/electrolyte interface, and hence contact loss between the plated Cu current collector and the HSE, is responsible for the very short cycle life. Figures 1b-d present SEM images showing the surface morphology of the fresh and cycled copper electrodes after plating 0.2 and 1 mAh/cm² at a current density of 0.05 mA/cm². After plating 0.2 mAh/cm², the smooth surface of copper is covered by a rough lithium-metal morphology (Figure 1c). The large and irregular-shaped lithium particles, having a diameter of $\sim 10 \mu m$, reflect a small density of nucleation centers, presumably initiated by the poor contact. After a deposition of 1 mAh/cm², the copper surface is covered by large lithium flakes with a diameter of >50 μ m. The lithium morphology in a solid-state Li-Cu battery is very different from that in liquid electrolyte-based batteries where mossy/dendritic lithium forms.²⁶ The large deposited lithium flakes in the solid-state battery appear to result in contact loss between the electrode and the HSE, also evidenced by easy removal of the current collector after disassembling, suggesting that more homogeneous plating on the copper surface is demanded.

Bare copper is not lithium-phobic, and, as a consequence, large deposited lithium flakes had a tendency to be formed, because of the insufficient active lithium-metal-grown sites. ZnO is known to improve the wettability of garnet solid-state electrolytes to molten lithium, because of a conversion reaction upon lithiation in the voltage range of 0–1 V vs Li/Li^{+.27,28} Here, we aim to use the resulting lithium-phillic Zn–Li alloy particles acting as nucleation seeds for lithium-metal growth upon subsequent plating at 0 V vs Li/Li⁺ on bare Cu, to achieve more homogeneous and thin lithium-metal growth, and thereby prevent delamination. Using ALD, a 100-nm thin film of ZnO is deposited on the surface of the copper current collector, as shown in Figure 2a, which is referred to as ZnO@Cu. To verify the thickness of ZnO, XPS depth profiling was

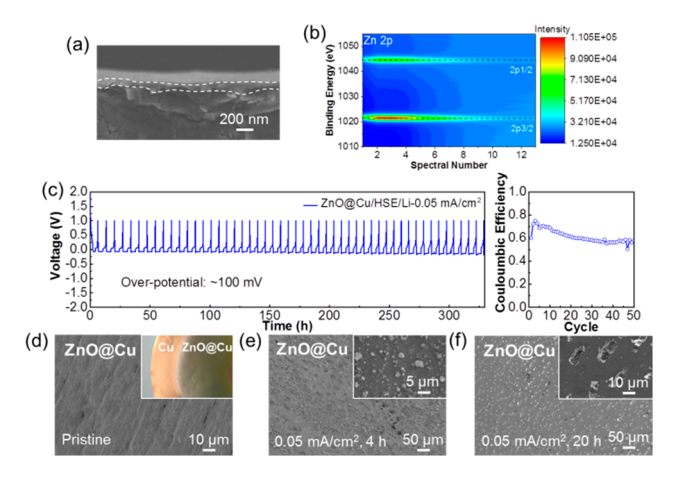


Figure 2. Plating lithium metal at the ZnO@Cu/HSE interface. (a) Cross-section SEM measurements showing the morphology of the ALD-deposited ZnO on a Cu current collector (ZnO@Cu). (b) Zn 2p XPS depth profile of the pristine ZnO@Cu current collector. (c) Electrochemical performance of the ZnO@Cu/HSE/Li battery at 0.05 mA/cm² for 4 h. (d, e, f) SEM images of the pristine ZnO@Cu current collector, the Li metal morphology after plating at 0.05 mA/cm² up to a capacity of 0.2 and 1 mAh/cm², respectively.

performed as shown in Figure 2b, where Zn 2p XPS signal is present until a depth of ~100 nm (each spectrum was taken after depth profiling every 10 nm). The voltage response upon cycling at 0.05 for 4 h is shown in Figure 1c. Comparing the cycling of the bare Cu current collector (Cu/HSE/Li battery), Figure 1a, with the cycling of the ZnO@Cu current collector (ZnO@Cu/HSE/Li battery) shows that the presence of the thin ZnO film results in a Li-Zn alloy formation platform at 0.5 V^{29,30} (Figure S1) and a significant decrease in the overpotential (~80 mV). In addition, the introduction of the ZnO thin film increases the Coulombic efficiency significantly (65%), as wel as the reversibility. Increasing the current density to 0.1 mA/cm² for 10 h during 10 cycles also results in relatively good performance with a Coulombic efficiency of \sim 75% (see Figure S2 in the Supporting Information). The morphology of the fresh ZnO@Cu and after Li metal deposition are presented in Figures 2d-f. As shown in the SEM images, the ALD-deposited ZnO film (Figure 2d) covers the wrinkled copper surface. As compared to the lithium deposits on bare copper (Figures 1c and 1d), the lithium-metal deposits on the ZnO@Cu current collector are isolated and much smaller, with a diameter of $\sim 3 \mu m$, after plating at 0.05 mA/cm² up to 0.2 mAh/cm², as shown in Figure 2e. The homogeneously distributed and isolated nature of the plated lithium-metal particles on the current collector are suggested to form because the Li-Zn alloy acts as seed crystal for lithium-metal nucleation. After plating up to 1 mAh/cm², the lithium-metal particles grow to an average size of \sim 10 μ m, which is much smaller and more regular-shaped, compared to the large lithium flakes when plating on the bare copper current collector in the Cu/HSE/Li battery. We conclude that the ZnO layer on the copper current collector, through the formation of well-distributed Zn-Li alloy particles, initiates the well-distributed and relatively monodisperse growth of lithium metal. This appears very beneficial for the lithium-metal plating/stripping reversibility, most likely because it enables a dissipated localized stress and maintains much better contact with the HSE, as indicated by the lower overpotentials.³¹ The impedance evolution for Cu/HSE/Li and ZnO@Cu/HSE/Li

batteries before and after five cycles are shown in Figure S3 in the Supporting Information. This demonstrates that the interfacial impedance of ZnO@Cu/HSE/Li is significantly smaller than Cu/HSE/Li after five cycles, which is consistent with better contact between the current collector and the HSE. To gain more insight in the reversibility of the lithium-metal plating/stripping behavior of the ZnO@Cu/HSE interface under operando conditions, NDP is employed as direct probe of the lithium-metal distribution, as a function of depth perpendicular to the current collector.

Neutron depth profiling (NDP) enables quantitative, non-destructive monitoring of the spatial distribution of lithium metal, perpendicular to the current collector, under realistic battery operation conditions. Thereby, it can provide valuable insights in the formation of the SEI and the evolution of the Li-concentration gradient associated with lithium-metal plating/stripping, and how these processes depend on the electrochemical conditions. Figure 3 shows the operando NDP

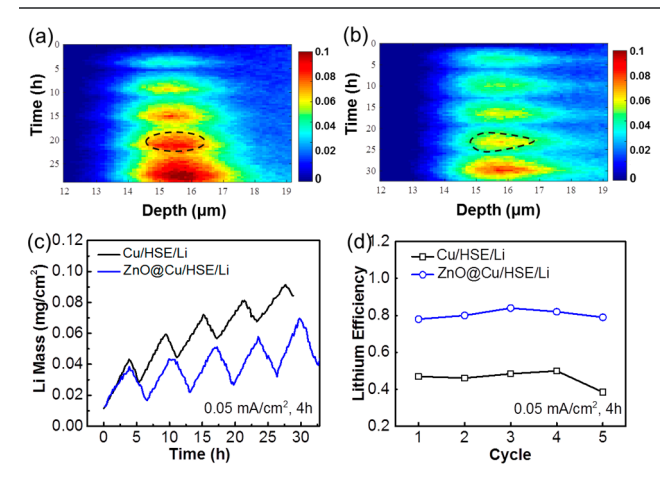


Figure 3. Impact of the ALD ZnO layer on Li density distribution in solid-state lithium copper battery. (a, b) Operando NDP measurements for five cycles of the Cu/HSE/Li and ZnO@Cu/HSE/Li batteries at 0.05 mA/cm². The color intensity quantifies the measured lithium density normalized to bulk lithium metal.(c, d) Lithium density and lithium efficiency evolution of Cu/HSE/Li and ZnO@Cu/HSE/Li batteries. The depth is measured from the outside surface of the copper; hence, the plating starts at $\sim\!12~\mu\text{m}$, representing the thickness of the copper current collector window. The color scale of the NDP measurements indicates the fractional Li density normalized to lithium metal.

results of the lithium-metal plating in the solid-state Cu/HSE/ Li and ZnO@Cu/HSE/Li batteries, yielding the normalized lithium-metal density (measured Li density normalized on the bulk lithium-metal density), as a function of depth, over five cycles at a current density of 0.05 mA/cm². The depth as shown in Figures 3a and 3b is measured, starting from the interface between the Cu current collector and the HSE (located at a depth of \sim 12 μ m). For the bare copper current collector in the Cu/HSE/Li battery, the average Li density, as well as the thickness of the deposits, rapidly increase upon cycling (Figure 3a), reflecting the buildup of inactive lithiummetal and Li-species at the HSE side overcycling. This is improved for the ZnO@Cu current collector, reflecting better affinity between the Li metal with the ZnO-covered current collector, and this is consistent with the improved electrochemical cycling shown in Figure 2c. Integrating the Li-density depth profiles in Figures 3a and 3b results in the evolution of

the plated lithium mass during cycling, as shown in Figure 3c for both the Cu/HSE/Li and ZnO@Cu/HSE/Li batteries. The total amount of inactive Li quantified by NDP is a combination of "dead" Li metal, and inactive Li in the SEI, since the chemical nature of Li cannot be distinguished with NDP. The ratio of the stripped capacity and the plated capacity represents the Li-efficiency, complementary to the Coulombic efficiency (electron efficiency). The presence of the ZnO film on the copper current collector raises the Li efficiency from ~45% to 80%, reflecting a more-efficient plating/stripping process (Figure 3d).

From the operando NDP results, probing the average Li density over ~1 cm² of the electrode, and the by SEM observed regular distributed and relatively monodisperse lithium-metal particles, we propose the process shown in Figure 4. In the Cu/HSE/Li battery (Figure 4a), the absence

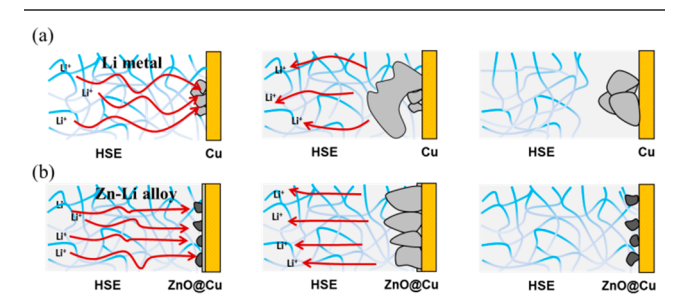


Figure 4. Schematic illustration for the lithium-metal plating/ stripping process on (a) a bare copper current collector and (b) a ZnO@Cu current collector.

of nucleation sites on the Li-phobic copper results in large, nonuniform lithium-metal flakes, as observed in Figures 1c and 1d. This can be expected to be a self-amplified process, because it induces a nonuniform Li-ion flux through the limited contact points between lithium metal and HSE. Upon stripping, this leads to effective delamination of the HSE, explaining the large voltage polarization observed in Figure 1a. In contrast, the conversion of the thin ZnO film toward Zn-Li alloy particles results in small nucleation sites for subsequent lithium-metal plating, as shown in Figures 2e and 2f, on the copper surface. The resulting homogeneous distribution of small lithium-metal particles will lead to more contact points with the HSE and, thus, a more homogeneous Li-ion flux distribution (Figure 4b). This suppresses delamination, and rationalizes the improved reversibility of the plating/stripping process, as observed with operando NDP.

Aiming at further improving the interface of the ZnO@Cu current collector with the HSE, the impact of prelithiation is investigated. After being prelithiated to 1 mAh/cm² Li, the ZnO@Cu/HSE/Li battery demonstrates stable cycling at 0.5 mAh/cm² with almost 100% Coulombic efficiency over 40 cycles.(Figures 5a and 5b) Clearly, this compromises the energy density as well as the full cell assembly conditions. The prelithiation may be optimized to yield much lower Li prelithiation capacities, which is the subject of further research. Here, we employ this approach to demonstrate cycling of the 1 mAh/cm² prelithiated ZnO@Cu in combination with a 3 mg/ cm² LiFePO₄ cathode. This full solid-state lithium-metal battery geometry delivers relatively stable cycling, at an average Coulombic efficiency of ~95%, as shown in Figures 5c and 5d. After 45 cycles, a capacity of ~100 mAh/g is still maintained (see Figure S4 in the Supporting Information), demonstrating

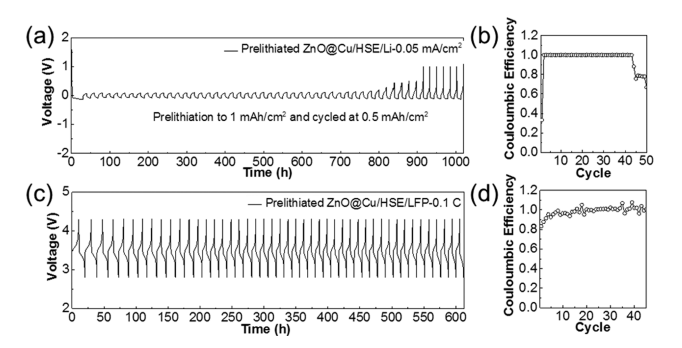


Figure 5. Full cells composed of prelithiated ZnO@Cu anode and LFP cathode. (a, b) Electrochemical performance of the ZnO@Cu/HSE/Li battery prelithiated to 1 mAh/cm² and cycled at 0.5 mAh/cm². (c, d) Electrochemical performance of the ZnO@Cu/HSE/LFP battery cycled at 0.1 C.

that the present lithium-metal current collector configuration shows perspective for full solid-state lithium-metal batteries.

In conclusion, cycling of solid electrolytes in combination with lithium-metal anodes is generally demonstrated starting with a thick lithium-metal anode. Ideally, the battery is assembled in its discharged state, without a major excess of lithium metal, hence, with the solid electrolyte directly facing the current collector. This is a much more challenging condition in practice, leading to severe delamination of the solid electrolyte from the current collector upon repeated lithium-metal plating/stripping, resulting in early cell death. Here, we explore a potential strategy to improve the HSE/Cu interface by introducing a 100-nm thin film of ZnO on the copper current collector, effectively making the current collector lithium-philic. The conversion reaction upon lithiation results in a regular distribution of small Zn-Li particles, acting as seed crystals for lithium-metal plating. A stable solid-state full cell composed of prelithiated ZnO@Cu cathode and LiFePO₄ cathode was demonstrated, providing insights in a potential route toward solid-state lithium-metal batteries.

EXPERIMENTAL SECTION

Hybrid solid electrolyte (HSE) films were prepared by mixing 0.768 g of PEO (Sigma-Aldrich, Mw = 600 000), 0.28 g of LiTFSI (Sigma-Aldrich), 0.403 g of SN (Sigma-Aldrich), and 0.105 g of LAGP (synthesized by conventional solid-state sintering method) together in 10 mL of acetonitrile (Sigma-Aldrich) and stirring for 24 h. The prepared solution was evenly casted on a Teflon plate and dried in the glove box at room temperature for 24 h. Detailed electrolyte property can be found in our previous literature. 14 The HSE-based all-solidstate cells were assembled in an argon-filled glove box. These cells consisted of lithium metal, Cu or ZnO@Cu and LiFePO4 as negative and positive electrodes, and the HSE electrolyte and separator layer. Charge-discharge tests of the HSE-based all-solid-state cells were performed using a Maccor 4000 battery cycler at 25 °C. Lithium-metal plating electrodes were prepared by discharging the cell for 0.2 mAh/cm² and 1 mAh/ cm² capacity. Subsequently, electrodes were transferred into a SEM (JEOL JSM-6010LA) system under dry argon conditions, and images were taken using an accelerating voltage of 10 kV. EIS measurements were performed from 100 kHz to 1 Hz, with an alternating current amplitude of 5 mV, using an Autolab (PGSTAT302N).

ZnO@Cu was prepared using the Spatial-ALD equipment at TNO-Holst Centre, which relies on the spatial, rather than the conventional temporal distribution of reagent precursors.³⁴ Depositions are performed at atmospheric pressure, while preserving the self-limiting nature of conventional ALD. In this work, a rotary type reactor was used, which allows up to 152mm round substrates to be mounted. More details on the reactor used can be found elsewhere.³⁵ Depositions were done by mounting copper foils on a holder and loaded them into the S-ALD reactor. The deposition precursors were diethylzinc (DEZ) and H₂O, each dosed at 50 and 500 sccm, respectively. The temperature of the precursor bottles was controlled outside the reactor and kept at room temperature for DEZ and 50 °C for H₂O. Depositions with a thickness of 100 nm were performed with 200 rpm substrate rotation frequency and a fixed substrate temperature of 200 °C.

A X-ray photoelectron spectrometer with Ar⁺ beam was employed to investigate the thickness of ALD ZnO on Cu (PHIS000 VersaProbe-II). The applied X-ray source was monochromatic K_{α} X-rays at 1486.6 eV (aluminum anode) under ultrahigh vacuum (10^{-9} Torr) conditions. The instrument work function was calibrated to give a binding energy (BE) of 83.96 eV for the Au $4f_{7/2}$ line on a metallic gold reference sample and the spectrometer dispersion was adjusted to give a BE of 932.62 eV for the Cu $2p_{3/2}$ line on a metallic copper sample. The depth-profiling sputtering was conducted by 2 min of sputtering in five cycles (2 kV, 2 mm × 2 mm), the narrow spectra of particular elements were recorded after each cycle of sputtering. The pass energy used for the hemispheric analyzer was 58.7 eV, and the base pressure of the system was $\sim 1 \times 10^{-7}$ Pa. The estimated sputtering rates are 5 nm/min.

Neutron depth profiling was performed on thermal neutron beamline A at the Reactor Institute Delft. The detailed setup and working principal can be found in our previous literature. To relate the triton ($^3H^+$) energy loss and intensity to the Li depth and Li density, the data must be corrected for the stopping power of the materials. The energy-dependent stopping power was calculated using SRIM (2013 version) 36 for the 12 μ m copper current collector (density = 8.96 g/cm 3), and for the electrolyte based on PEO (density = 1.21 g/cm 3), SN (density = 0.985 g/cm 3), LiTFSI (density = 1.33 g/cm 3), and LAGP (density = 3.42 g/cm 3).

■ ASSOCIATED CONTENT

Supporting Information

The Supporting Information is available free of charge at https://pubs.acs.org/doi/10.1021/acsmaterialslett.0c00152.

Initial discharge curves and impedance evolution for Cu/HSE/Li and ZnO@Cu/HSE/Li batteries; initial capacity-voltage profiles of the ZnO@Cu/HSE/LFP battery (PDF)

AUTHOR INFORMATION

Corresponding Author

Marnix Wagemaker — Section Storage of Electrochemical Energy, Radiation Science and Technology, Faculty of Applied Sciences, Delft University of Technology, 2628, CD, Delft, The Netherlands; ⊚ orcid.org/0000-0003-3851-1044; Email: m.wagemaker@tudelft.nl

Authors

- Ming Liu Section Storage of Electrochemical Energy, Radiation Science and Technology, Faculty of Applied Sciences, Delft University of Technology, 2628, CD, Delft, The Netherlands
- Chao Wang Section Storage of Electrochemical Energy, Radiation Science and Technology, Faculty of Applied Sciences, Delft University of Technology, 2628, CD, Delft, The Netherlands
- Zhu Cheng Section Storage of Electrochemical Energy, Radiation Science and Technology, Faculty of Applied Sciences, Delft University of Technology, 2628, CD, Delft, The Netherlands
- Swapna Ganapathy Section Storage of Electrochemical Energy, Radiation Science and Technology, Faculty of Applied Sciences, Delft University of Technology, 2628, CD, Delft, The Netherlands
- Lucas A. Haverkate TNO-Holst Centre, Dutch National Institute for Applied Scientific Research, 5656, AE, Eindhoven, The Netherlands
- Sandeep Unnikrishnan TNO-Holst Centre, Dutch National Institute for Applied Scientific Research, 5656, AE, Eindhoven, The Netherlands

Complete contact information is available at: https://pubs.acs.org/10.1021/acsmaterialslett.0c00152

Author Contributions

 ${}^{
abla}$ These authors contributed equally to this work.

Notes

The authors declare no competing financial interest.

ACKNOWLEDGMENTS

The authors thank Michel Steenvoorden, and Frans Ooms for their assistance with experiments. M.L. acknowledges support by the Netherlands Organization for Scientific Research (NWO) (under Grant No. 15788), and M.W. was supported under the VICI (Grant No. 16122). Financial support from the Advanced Dutch Energy Materials (ADEM) program of the Dutch Ministry of Economic Affairs, Agriculture and Innovation is gratefully acknowledged. C.W. would like to thank the Guangzhou Elite Project for financially supporting part of the work in this paper.

REFERENCES

- (1) Whittingham, M. S. Electrical energy storage and intercalation chemistry. *Science* **1976**, *192*, 1126–1127.
- (2) Lin, D.; Liu, Y.; Cui, Y. Reviving the lithium metal anode for high-energy batteries. *Nat. Nanotechnol.* **2017**, *12*, 194–201.
- (3) Cheng, X.; Zhang, R.; Zhao, C.; Zhang, Q. Toward Safe Lithium Metal Anode in Rechargeable Batteries: A Review. *Chem. Rev.* **2017**, 117, 10403–10473.
- (4) Luntz, A. C.; McCloskey, B. D. Nonaqueous Li-air batteries: a status report. *Chem. Rev.* **2014**, *114*, 11721-11750.
- (5) Manthiram, A.; Fu, Y.; Chung, S.; Zu, C.; Su, Y. Rechargeable lithium—sulfur batteries. *Chem. Rev.* **2014**, *114*, 11751–11787.
- (6) Liu, M.; Qin, X.; He, Y.; Li, B.; Kang, F. Recent innovative configurations in high-energy lithium—sulfur batteries. *J. Mater. Chem.* A **2017**, *5*, 5222—5234.
- (7) Aurbach, D.; Zinigrad, E.; Cohen, Y.; Teller, H. A short review of failure mechanisms of lithium metal and lithiated graphite anodes in liquid electrolyte solutions. *Solid State Ionics* **2002**, *148*, 405–416.
- (8) Bai, P.; Li, J.; Brushett, F. R.; Bazant, M. Z. Transition of lithium growth mechanisms in liquid electrolytes. *Energy Environ. Sci.* **2016**, *9*, 3221–3229.

- (9) Ngai, K. S.; Ramesh, S.; Ramesh, K.; Juan, J. C. A review of polymer electrolytes: fundamental, approaches and applications. *Ionics* **2016**, 22, 1259–1279.
- (10) Yao, X.; Huang, B.; Yin, J.; Peng, G.; Huang, Z.; Gao, C.; Liu, D.; Xu, X. All-solid-state lithium batteries with inorganic solid electrolytes: Review of fundamental science. *Chin. Phys. B* **2016**, 25, 018802.
- (11) Quartarone, E.; Mustarelli, P. Electrolytes for solid-state lithium rechargeable batteries: recent advances and perspectives. *Chem. Soc. Rev.* **2011**, *40*, 2525–2540.
- (12) Yang, C.; Zhang, L.; Liu, B.; Xu, S.; Hamann, T.; McOwen, D.; Dai, J.; Luo, W.; Gong, Y.; Wachsman, E. D.; Hu, L. Continuous plating/stripping behavior of solid-state lithium metal anode in a 3D ion-conductive framework. *Proc. Natl. Acad. Sci. U. S. A.* **2018**, *115*, 3770–3775.
- (13) Zeng, X.; Yin, Y.; Li, N.; Du, W.; Guo, Y.; Wan, L. Reshaping lithium plating/stripping behavior via bifunctional polymer electrolyte for room-temperature solid Li metal batteries. *J. Am. Chem. Soc.* **2016**, 138, 15825–15828.
- (14) Liu, M.; Cheng, Z.; Ganapathy, S.; Wang, C.; Haverkate, I.; Tulodziecki, M.; Unnikrishnan, S.; Wagemaker, M. Tandem Interface and Bulk Li-ion Transport in a Hybrid Solid Electrolyte with Micro-Sized Active Filler. ACS Energy Lett. 2019, 4, 2336–2342.
- (15) Yue, L.; Ma, J.; Zhang, J.; Zhao, J.; Dong, S.; Liu, Z.; Cui, G.; Chen, L. All solid-state polymer electrolytes for high-performance lithium ion batteries. *Energy Storage Mater.* **2016**, *5*, 139–164.
- (16) Zheng, J.; Gu, M.; Chen, H.; Meduri, P.; Engelhard, M. H.; Zhang, J.; Liu, J.; Xiao, J. Ionic liquid-enhanced solid state electrolyte interface (SEI) for lithium—sulfur batteries. *J. Mater. Chem. A* **2013**, *1*, 8464—8470.
- (17) Xu, K. Electrolytes and interphases in Li-ion batteries and beyond. Chem. Rev. 2014, 114, 11503-11618.
- (18) Bachman, J. C.; Muy, S.; Grimaud, A.; Chang, H.-H.; Pour, N.; Lux, S. F.; Paschos, O.; Maglia, F.; Lupart, S.; Lamp, P.; Giordano, L.; Shao-Horn, Y. Inorganic Solid-State Electrolytes for Lithium Batteries: Mechanisms and Properties Governing Ion Conduction. *Chem. Rev.* **2016**, *116*, 140–162.
- (19) Zhang, H.; Li, C.; Piszcz, M.; Coya, E.; Rojo, T.; Rodriguez-Martinez, L. M.; Armand, M.; Zhou, Z. Single lithium-ion conducting solid polymer electrolytes: Advances and perspectives. *Chem. Soc. Rev.* **2017**, *46*, 797–815.
- (20) Goodenough, J. B.; Singh, P. Review-Solid electrolytes in rechargeable electrochemical cells. *J. Electrochem. Soc.* **2015**, *162*, A2387—A2392.
- (21) Shim, J.; Kim, L.; Kim, H. J.; Jeong, D.; Lee, J. H.; Lee, J. All-solid-state lithium metal battery with solid polymer electrolytes based on polysiloxane crosslinked by modified natural gallic acid. *Polymer* **2017**, *122*, 222–231.
- (22) Kotobuki, M.; Kanamura, K.; Sato, Y.; Yoshida, T. Fabrication of all-solid-state lithium battery with lithium metal anode using Al₂O₃-added Li₇La₃Zr₂O₁₂ solid electrolyte. *J. Power Sources* **2011**, 196, 7750–7754.
- (23) Han, X.; Gong, Y.; Fu, K. K.; He, X.; Hitz, G. T.; Dai, J.; Pearse, A.; Liu, B.; Wang, H.; Rubloff, G.; et al. Negating interfacial impedance in garnet-based solid-state Li metal batteries. *Nat. Mater.* **2017**, *16*, 572–579.
- (24) Yun, Q.; He, Y.; Lv, W.; Zhao, Y.; Li, B.; Kang, F.; Yang, Q. Chemical dealloying derived 3D porous current collector for Li metal anodes. *Adv. Mater.* **2016**, 28, 6932–6939.
- (25) Zhang, J.-G. Anode-less. Nat. Energy 2019, 4, 637-638.
- (26) Shi, Q.; Zhong, Y.; Wu, M.; Wang, H.; Wang, H. High-capacity rechargeable batteries based on deeply cyclable lithium metal anodes. *Proc. Natl. Acad. Sci. U. S. A.* **2018**, *115*, 5676–5680.
- (27) Yang, C.; Fu, K.; Zhang, Y.; Hitz, E.; Hu, L. Protected Lithium-Metal Anodes in Batteries: From Liquid to Solid. *Adv. Mater.* **2017**, 29, 1701169.
- (28) Wang, C.; Gong, Y.; Liu, B.; Fu, K.; Yao, Y.; Hitz, E.; Li, Y.; Dai, J.; Xu, S.; Luo, W.; Wachsman, E. D.; Hu, L. Conformal,

- nanoscale ZnO surface modification of garnet-based solid-state electrolyte for lithium metal anodes. *Nano Lett.* **2017**, *17*, 565–571.
- (29) Xie, Q.; Zhang, X.; Wu, X.; Wu, H.; Liu, X.; Yue, G.; Yang, Y.; Peng, D. Yolk-shell ZnO-C microspheres with enhanced electrochemical performance as anode material for lithium ion batteries. *Electrochim. Acta* **2014**, *125*, 659–665.
- (30) Zhang, G.; Hou, S.; Zhang, H.; Zeng, W.; Yan, F.; Li, C. C.; Duan, H. High-performance and ultra-stable lithium-ion batteries based on MOF-derived ZnO@ ZnO quantum Dots/C core—shell nanorod arrays on a carbon cloth anode. *Adv. Mater.* **2015**, 27, 2400—2405
- (31) Zhang, X.; Xiang, Q.; Tang, S.; Wang, A.; Liu, X.; Luo, J. Long Cycling Life Solid-State Li Metal Batteries with Stress Self-Adapted Li/Garnet Interface. *Nano Lett.* **2020**, *20*, 2871–2878.
- (32) Lv, S.; Verhallen, T.; Vasileiadis, A.; Ooms, F.; Xu, Y.; Li, Z.; Li, Z.; Wagemaker, M. Operando monitoring the lithium spatial distribution of lithium metal anodes. *Nat. Commun.* **2018**, *9*, 1–12.
- (33) Liu, M.; Cheng, Z.; Qian, K.; Verhallen, T.; Wang, C.; Wagemaker, M. Efficient Li-metal plating/stripping in carbonate electrolytes using a LiNO₃-gel polymer electrolyte, monitored by operando neutron depth profiling. *Chem. Mater.* **2019**, *31*, 4564–4574.
- (34) Poodt, P.; Cameron, D. C.; Dickey, E.; George, S. M.; Kuznetsov, V.; Parsons, G. N.; Roozeboom, F.; Sundaram, G.; Vermeer, A. Spatial atomic layer deposition: A route towards further industrialization of atomic layer deposition. *J. Vac. Sci. Technol., A* **2012**, *30*, 010802.
- (35) Illiberi, A.; Roozeboom, F.; Poodt, P. Spatial atomic layer deposition of zinc oxide thin films. *ACS Appl. Mater. Interfaces* **2012**, 4, 268–271.
- (36) Nagpure, S. C.; Downing, R. G.; Bhushan, B.; Babu, S. S. Discovery of lithium in copper current collectors used in batteries. *Scr. Mater.* **2012**, *67*, 669–672.